Erratum

The importance of leading edge vortices under simplified flapping flight conditions at the size scale of birds

Tatjana Y. Hubel and Cameron Tropea

10.1242/jeb.047886

There was an error published in *J. Exp. Biol.* **213**, 1930-1939.

In the PDF and print versions of the article, the top of Fig. 6 was inadvertently cropped. The Full Text version of the article is not affected by this error.

The correct (uncropped) version of the figure is shown below.

We apologise to authors and readers for this mistake.

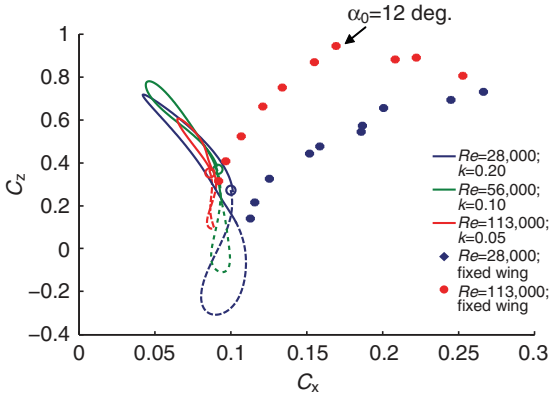

The Journal of Experimental Biology 213, 1930-1939

doi:10.1242/jeb.040857

The importance of leading edge vortices under simplified flapping flight conditions at the size scale of birds

Tatjana Y. Hubel* and Cameron Tropea

Fachgebiet Strömungslehre und Aerodynamik, Technische Universität Darmstadt, 64287, Germany

*Author for correspondence at present address: Structure and Motion Laboratory, The Royal Veterinary College, North Mymms, Hatfield, Hertfordshire AL9 7TA, UK (thubel@rvc.ac.uk)

Accepted 21 February 2010

SUMMARY

Over the last decade, interest in animal flight has grown, in part due to the possible use of flapping propulsion for micro air vehicles. The importance of unsteady lift-enhancing mechanisms in insect flight has been recognized, but unsteady effects were generally thought to be absent for the flapping flight of larger animals. Only recently has the existence of LEVs (leading edge vortices) in small vertebrates such as swifts, small bats and hummingbirds been confirmed. To study the relevance of unsteady effects at the scale of large birds [reduced frequency k between 0.05 and 0.3, $k=(\pi fc)/U_\infty$; f is wingbeat frequency, U_∞ is free-stream velocity, and c is the average wing chord], and the consequences of the lack of kinematic and morphological refinements, we have designed a simplified goose-sized flapping model for wind tunnel testing. The 2-D flow patterns along the wing span were quantitatively visualized using particle image velocimetry (PIV), and a three-component balance was used to measure the forces generated by the wings. The flow visualization on the wing showed the appearance of LEVs, which is typically associated with a delayed stall effect, and the transition into flow separation. Also, the influence of the delayed stall and flow separation was clearly visible in measurements of instantaneous net force over the wingbeat cycle. Here, we show that, even at reduced frequencies as low as those of large bird flight, unsteady effects are present and non-negligible and have to be addressed by kinematic and morphological adaptations.

Key words: leading edge vortex, bird flight, delayed stall.

INTRODUCTION

Studies of animal flight have attained a new level of detail over the last decade, due to a tremendous progress in measurement techniques and heightened interest in flapping flight among the academic, military and industrial spheres. This interest is, for the most part, inspired by the very high maneuverability allowed by flapping flight compared with conventional propulsion systems. Initially, the focus was primarily on insect flight (Ellington et al., 1996; van den Berg and Ellington, 1997; Willmott et al., 1997; Ellington, 1999). These early studies demonstrated that flow behavior at the size, speed and flapping frequency of insects is distinctly different from well-studied aeroplane aerodynamics. For example, flapping wings possess mechanisms of lift generation beyond those of fixed wings, such as wake capture, rotational lift and delayed stall, and these unsteady effects have been found to provide a substantial portion of the lift during insect flight (Dickinson et al., 1999; Sane, 2003). Interest in bird and bat flight has increased significantly over the last few years and with it the desire to understand vertebrate flight in its full complexity. Beyond experimental investigations and calculations regarding the wake pattern and aerodynamic forces (Hedrick et al., 2002; Spedding et al., 2003; Hedenström et al., 2006; Hedenström et al., 2007; Hubel et al., 2009), there is an increasing interest in complementary issues, such as power consumption (Rayner, 1999; Tobalske et al., 2003), maneuverability (Tobalske et al., 2007; Iriarte-Diaz and Swartz, 2008; Hedrick et al., 2009), kinematics (Hedrick et al., 2004; Riskin et al., 2008) and wing structure (Swartz et al., 1996; Swartz and Middleton, 2008), as well as the correlation of the morphological and physiological conditions, kinematics and generated aerodynamic forces (Rosen et al., 2004; Swartz et al., 2007; Tobalske, 2007).

Traditionally, vertebrate flight, unlike insect flight, has been assumed to exclude unsteady effects due to the much larger Reynolds number (*Re*) regime; however, recent work has shown that leading edge vortices (LEVs) also play a role in lift generation in the flight of small vertebrates. Well before this was revealed for in insect flight, LEVs have been known to contribute to lift generation in technical applications such as delta-winged aeroplanes operating at much higher Reynolds numbers than any animals. Contrary to conventional wings, where high angles of attack lead to stall and decreasing lift generation, these swept wings with a sharp leading edge take advantage of controlled stall conditions and flow reattachment on the upper surface (LEV), generating high lift and drag at high angles of attack (Videler, 2005). Studies on a fixed model swift wing show that swifts under gliding conditions are probably capable of developing stable LEV conditions (Videler et al., 2004). However, additional studies on real wings confirm the presence of a LEV but contradict additional lift gain (Lentink et al., 2007) and the direct analogy between LEVs on swept and flapping wings (Lentink and Dickinson, 2009).

Recent work has shown that LEVs are not limited to swift wings and gliding conditions. So far they have been observed on flapping wings of small (<10 g) bats (Muijres et al., 2008) and in hummingbird flight (Altshuler et al., 2004; Warrick et al., 2005; Warrick et al., 2009). This raises the question of whether the previous quasi-steady approach of bird flight might have to be reconsidered. Comparatively little is known about the influence of unsteady mechanisms over the wide range of Reynolds numbers and reduced

frequencies (k) typical of the flight of birds and large insects. However, steady flow conditions have often been assumed for reduced frequencies below 0.3 (Spedding, 1993). Despite the detailed studies of LEVs in insect flight many questions such as the source of LEV stability are still being discussed. Recent work shows the importance of wing deformation on the aerodynamic performance (Young et al., 2009; Zhao et al., 2009), contradicting earlier assumptions about rigid wing applicability for insect flight. The importance of the compliance in bat and bird wings is largely recognized but not comprehensively understood. Nevertheless, simplified rigid wings have often been used in experiments and simulations, in part justifiable by the very scarce amount of knowledge overall about the flow conditions around flapping wings in the vertebrate flight regime. Should unsteady effects, such as LEVs, be shown to be of potential importance under vertebrate flight conditions, one then has to introduce morphological and kinematic aerodynamic adaptations mimicking more realistically actual flight conditions, but with continued focus on not only flow separation but also LEV developments.

To gain a better understanding of the forces generated over the wingbeat cycle and potential consequences of non-exact kinematic and morphological refinements, we designed and built a simplified flapping wing model with goose-like body proportions operating in a range of k=0.05–0.3 and Re=28,000–113,000 (Hubel and Tropea, 2009). The manufactured wings were based on basic bird characteristic features. The model was investigated in a large low-speed wind tunnel. Measurements using a three-component force balance were used to determine the instantaneous forces (Hubel and Tropea, 2009). Results from these studies suggested additional lift generation based on unsteady effects, due to the movement of the wings. In this study we describe visualizations of the wing vortices from those experiments, in order to test the hypothesis that lift was generated by a LEV over the wingbeat cycle. We use particle image velocimetry (PIV) to visualize and quantify the flow conditions around the wing on several positions along the span.

MATERIALS AND METHODS

The model (Fig. 1) was inspired by the flight parameters and wing morphology typical of goose flight. The size of geese species varies considerably and ranges from wing spans of 0.9 m up to more than 2 m. Our model was based on the morphology of smaller species such as *Branta bernicular* and *Branta leucopsis* with wing spans between 1.1 m and 1.38 m and aspect ratios reported to be between 8 and 10 (Green and Alerstam, 2000; Lee et al., 2008). Flapping frequencies between 3.8 and 4.7 have been observed for *B. leucopsis* and flight speeds of 17–18 m s^{-1} have been measured during migration (Butler and Woakes, 1980; Green and Alerstam, 2000; Lee et al., 2008). Based on the given information the Reynolds number and reduced frequencies the birds are operating in can be assumed to be between Re=110,000–200,000 and k=0.07–0.15.

The model had a maximum flapping frequency of 2.2 Hz; a wing span of 1.13 m and an average wing chord of 0.141 m. The wing span in the lower range was chosen in order to avoid any possible wall effects in the closed-loop, low-speed wind tunnel (test section 2.90 m width × 2.20 m height × 4.90 m length, turbulence level <1%). To accommodate force balance requirements and mechanical limitations, measurements were restricted to Reynolds numbers between 28,000 and 133,000 in order to still obtain similar reduced frequencies as in bird flight.

The flapping motion was asymmetrical, with a downwards extension of 17 deg. and an upwards extension of 27 deg. The wings had a negative sweep of –7 deg. in the arm portion (41% of the wing) and a positive sweep of 10 deg. in the hand portion of the wing (59%). Flapping amplitude, wing geometry and sweep angles (at mid-downstroke) were extracted from video footage in 'Winged Migration' (Perrin, 2001) and 'Voisin des nuages avec les oies sauvages' (Cuvelier, 2000). The wing profile was based on a standard airfoil (Wortmann FX 60-126), representing the chamber, thickness and round leading edge typical for a bird wing arm portion.

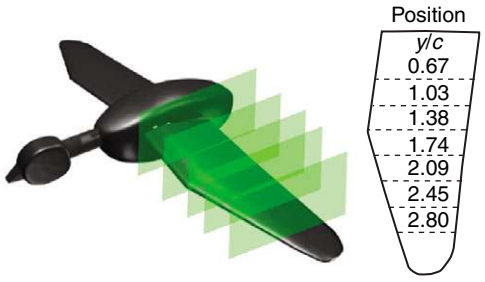

Fig. 1. Flapping wing model with visualization planes (schematic) and measurement positions along the span.

The movement of the wings was restricted to one degree of freedom without the implementation of any long axis rotation (twist), resulting in the lack of spanwise variable incidence. Highly rigid wings with a constant profile over the entire span restricted the model to simple flapping flight kinematics, lacking any kinematic and morphological refinements typically observed in insect and bird flight. The high rigidity and constant profile also simplified the manufacturing process and accompanying numerical calculations. The static angle of attack (α_0) at the shoulder joint could be varied manually between –2 deg. and +18 deg. for static measurements, but were restricted to +12 deg. under flapping conditions. The change in the static angle of attack was coupled with a simultaneous change in stroke plane angle due to the internal mechanics of the model. Further details are described in Hubel and Tropea (Hubel and Tropea, 2009).

An internal three-component balance was used to record the phase-related vertical force, horizontal force and pitching moment [measurement rates between 300 Hz and 600 Hz, measurement range (r) and precision (p): vertical force (r=±115 N, p=0.02%), horizontal force (r=±40.5 N, p=0.6%), pitching moment (r=±5.3 N m, p=1.5%)]. Direct force measurements are able to track the development of the force generation over the entire wingbeat cycle. To compare the forces generated by flapping wings with those on the wing under steady flow conditions, the wings were set in the fixed horizontal position and the forces measured at different static angles of attack and Reynolds numbers. To eliminate the contributions of the dynamic forces and added mass from the total forces experienced under flapping wing conditions, additional measurements without wind were performed for each test case, and subsequently subtracted from the test results obtained under 'wind on' conditions. It was assumed that the difference in mechanical and inertial forces for loaded ('wind on') and unloaded ('wind off') wing conditions is negligible [for further details, see Hubel and Tropea (Hubel and Tropea, 2009)].

A 10 Hz Butterworth low-pass filter was used to remove energy associated with the natural frequencies of the balance and wings. The recorded forces were partitioned into up- and downstroke and interpolated over the amplitude angle in order to gain an average over 10–15 wingbeat cycles. Subsequently, vertical (C_z), horizontal (C_x) and pitching (C_m) coefficients were calculated from the

averaged forces and moment. In contrast to the constant angle of attack for fixed wings, the effective angle of attack (α_{eff}) of flapping wings is a result of both horizontal and vertical flow due to the wing motion and changes over the wingbeat cycle as well as along the span. In order to compare the fixed and flapping wing results, the vertical force coefficient (C_z) was examined as a function of the effective angle of attack. Neglecting the induced angle of attack (α_{ind}) due to the downwash, the effective angle of attack was assumed to be equal to the static angle of attack for fixed wings in the horizontal position, while for flapping wings, the effective angle of attack was calculated at the mid-wing position considering the horizontal free-stream velocity ($\mathbf{U}_\infty$), the vertical component of wing velocity ($\mathbf{v}_z$) at mid-wing position and the static angle of attack:

$$\alpha_{eff}(t) = \alpha_0 + \arctan\frac{\mathbf{v}_z(t)}{\mathbf{U}_\infty}, \quad (1)$$

where α_0 is the static angle of attack at the shoulder joint, t is time, and where we obtained the instantaneous vertical velocity ($\mathbf{v}_z$) *via* a rotational potentiometer on the shoulder joint. The influence of the vertical wing velocity on the effective angle of attack along the span is displayed in Fig. 2 for k=0.1–0.3. The lack of spanwise variable incidence in the model results in a linear increase of the effective angle of attack contrary to real bird wings that may exhibit a more constant of angle of attack due to the geometrical twist along the span (Bilo, 1971; Bilo and Nachtigall, 1977).

A 2-D PIV system [200 mJ Nd:YAG double-pulse laser (10 Hz), PCO SensiCam, 1024×1280 pixels, seeding: di-ethyl-hexyl-sebacate (DEHS), Palas, Karlsruhe, Germany] was used to capture the instantaneous velocity field on the wing parallel to the flow stream (Fig. 3). Measurements at seven positions along the span (Fig. 1) were performed. The instantaneous vector field was calculated by using the adaptive correlation function in the Dantec Dynamics software (FlowManager®, Dantec Dynamics A/S, Skovlunde, Denmark). The interrogation area was 32×32 pixels with a 50% overlap, and outlying vectors were eliminated by a local neighborhood validation with a vector area of 3×3 pixels. Masks were generated for the wing area and for areas in the wing shadow without valid PIV information. The obstruction by the surface of the wing results in limited views of the upper and lower wing surface during the wingbeat cycle. The cameras were positioned parallel to the wing in its horizontal position in order

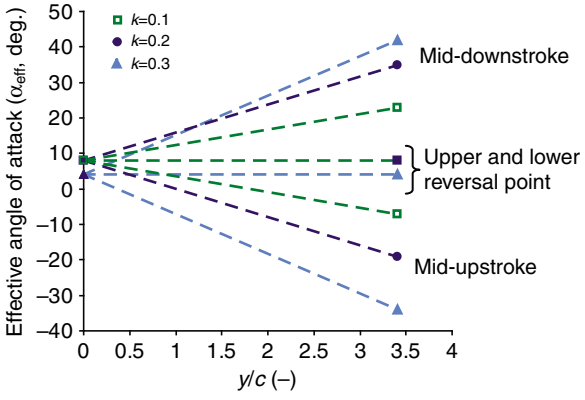

Fig. 2. Change in effective angle of attack along the span at k=0.1, 0.2, 0.3 for α_0=4 deg. (k=0.3) and 8 deg. (k=0.1, k=0.2); k, reduced frequency; α_0, static angle of attack.

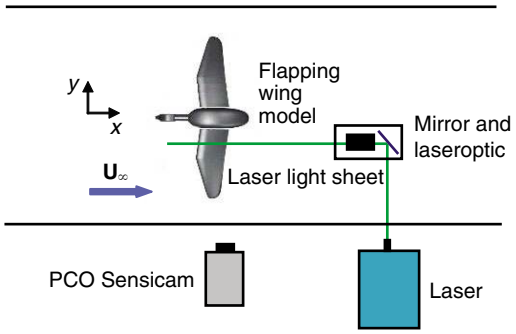

Fig. 3. Top view of the experimental set-up. $\mathbf{U}_\infty$, free-stream velocity.

to optimize the view at this phase of the wingbeat cycle. This position was chosen because the vertical wing velocity (hence, the effective angle of attack) was maximum close to mid-downstroke, and it was therefore likely to exhibit different flow conditions along the span. Although the wings were black in order to reduce laser reflections, near-wall reflections, as well as limitations in the resolution due to the size of the observation area, led to limited information in the immediate near-wall area. The reflections were strongly dependent on the wing position over the phase of the wingbeat cycle and angle of attack, with the least reflection generated near the horizontal position. However, even under good conditions, no flow information could be gained closer than 3 mm to the surface, this preventing the resolution of the boundary layer itself. In the data presented, the mean velocity was removed to better visualize the unsteady vortex structure above the wing. To distinguish between a LEV and other separation phenomena, a LEV is defined by the detection of reverse flow whereas other reattaching flow is defined as a separation bubble. Cases without flow reattachment are classified as fully separated flows.

PIV measurements were conducted at Reynolds numbers between 28,000 and 113,000 and through a range of reduced frequencies between 0.05 and 0.3. A static angle of attack of 8 deg. was chosen in order to achieve effective angles of attack exceeding the critical angle of attack for fixed wings for a flapping frequency of 1.3 Hz. Additional measurements with α_0=4 deg. and a flapping frequency of 2 Hz were also performed. Force measurements were conducted for different static angles of attack but limited to a range of k=0.05–0.2 in flapping flight in order to prevent any damage to the force balance due to high peaks in force at the reversal points.

RESULTS

Fig. 4 shows the result of the quasi-steady measurements for wings fixed in a horizontal position at different Reynolds numbers and static angles of attack. Vertical force coefficients for Re=28,000 were distinctly lower, differences at higher Reynolds numbers were small, although measurable. The lift coefficients at the higher Reynolds numbers were in good agreement with 3-D values calculated using data from a 2-D Wortmann Fx 60-126 airfoil (Althaus, 1981) and extended to 3-D using lifting line theory. The comparison with measurements taken at Re=113,000 showed a discrepancy of less than 6% in vertical force coefficients for static angles of attack between 2 deg. and 14 deg.

Vertical force coefficient changed throughout the wingbeat cycle. At a pre-selected static angle of attack of 8 deg. and subsequently

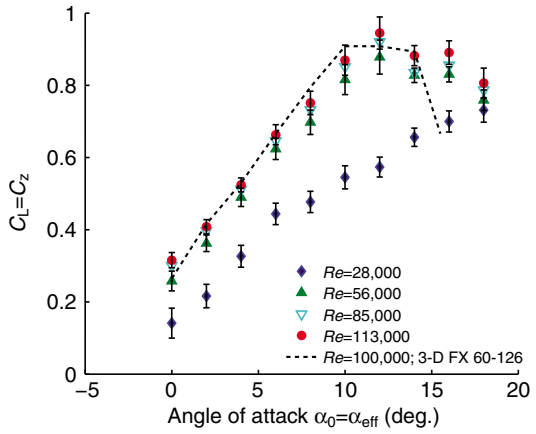

Fig. 4. Vertical force coefficient (C_z) *versus* angle of attack for the wings fixed in horizontal position, at different Reynolds numbers (*Re*) compared with a 3-D Wortmann Fx 60-126 airfoil (Althaus, 1981). In case of the fixed wings the C_z is equal to the lift coefficient (C_L), and the static angle of attack (α_0), adjusted at the shoulder joint, is constant along the span and equal to the effective angle of attack (α_{eff}), neglecting the induced angle of attack.

relatively high effective angles of attack, vertical force coefficient exceeded the maximum force coefficient for fixed wings ($C_{z\_max\_fixed}$) at all Reynolds numbers, most obviously at *Re*=56,000 and 28,000 (Fig. 5). In addition there were significant differences in the vertical force coefficient values at the same effective angles of attack throughout the wingbeat cycle for *Re*=28,000, 56,000 and 86,000 (not displayed), as well as during the upstroke for *Re*=113,000.

The thrust generation due to the wing motion was evident in the comparison of vertical force coefficient *versus* horizontal force

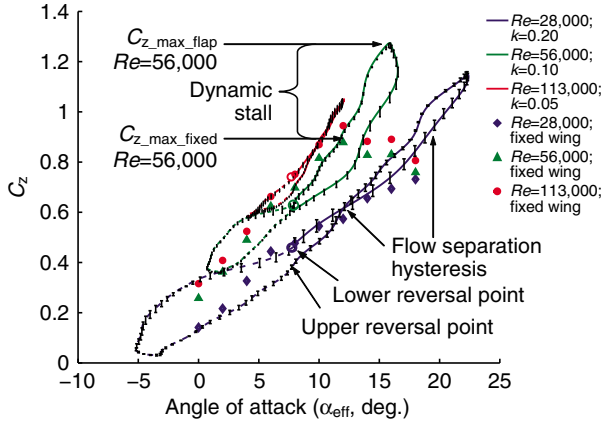

Fig. 5. Vertical force coefficient (C_z) *versus* effective angle of attack (α_{eff}) for fixed wings in comparison with the results of flapping wings at different Reynolds numbers (*Re*) and reduced frequencies (*k*) [*f*=1.28 Hz, α_0=8 deg., α_{eff} calculated at mid-wing position, (o) lower reversal point, (- - -) upstroke, (—) downstroke]. The flapping wing results show the following unsteady effects: the critical angle of attack for fixed wings is exceeded (at $C_{z\_max\_fixed}$), indicating dynamic stall; different C_z values at identical α_{eff} (indicating aerodynamic phase lag) and a rapid drop in C_z at high α_{eff} (indicating flow separation) with long delays in reattachment (hysteresis). These effects are especially pronounced at reduced frequencies $k \geq 0.07$, but even at *k*=0.05 the maximum C_z for fixed wings is exceeded.

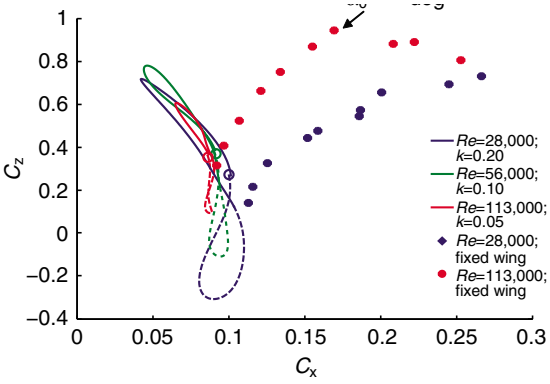

Fig. 6. Vertical force coefficient (C_z) *versus* horizontal force coefficient (C_x) at different Reynolds numbers (*Re*) in comparison with fixed wings results. [α_0=0 deg., (o) lower reversal point, (- - -) upstroke, (—) downstroke]. α_0, static angle of attack.

coefficient for fixed and flapping wings (Fig. 6). The polar curve for fixed wings showed the typical increase in lift and drag at increasing angle of attack. The fixed wings showed a rapid decrease in lift-to-drag ratio at higher angles of attack (*Re*>=56,000), indicating that the critical angle of attack was exceeded and the onset of stall conditions at α_0=12 deg. has occurred. At *Re*=28,000 the lift-to-drag ratio was clearly smaller and the transition into stall occurred more gradually. While the thrust generated by the flapping wings was insufficient in overcoming the drag generated by the mechanical model, significant reduction in the drag coefficients during the entire downstroke for all Reynolds numbers at α_0=0 deg. was observed. At a constant Reynolds number, increasing effective angles of attack due to an increase of static angles of attack were accompanied by decreasing lift-to-drag ratios during the downstroke (Fig. 7). Vertical force coefficient values clearly exceeded the maximum lift coefficient for fixed wings, and horizontal force coefficient values showed an additional rapid increase approaching the mid-downstroke position.

Flow fields were measured at different spanwise locations over the lower part of the wingbeat cycle starting as the wing passed through the horizontal position during the downstroke. The flow on the wing revealed different flow conditions and transitions

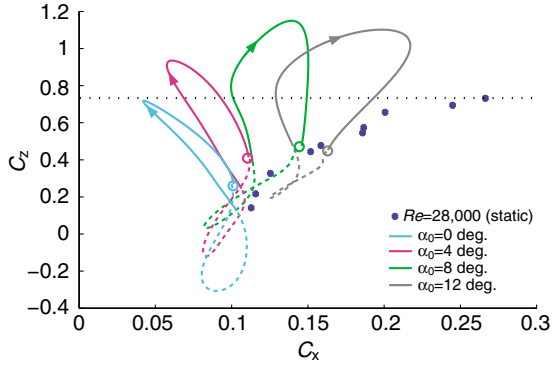

Fig. 7. Vertical force coefficient (C_z) *versus* horizontal force coefficient (C_x) at different static angles of attack (α_0) in comparison with fixed wings results. [*Re*=28,000; *k*=0.20, dashed black line indicates the maximum force coefficient for fixed wings ($C_{z\_max\_fixed}$)]; (o) lower reversal point, (- - -) upstroke, (—) downstroke).

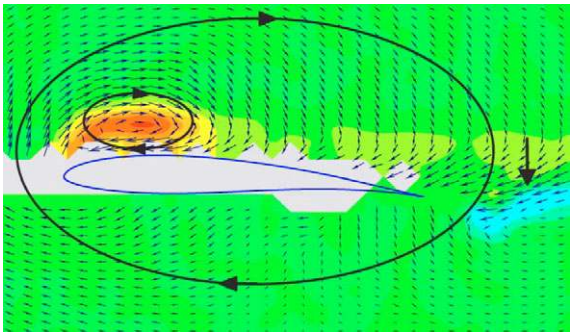

Fig. 8. Vector field after subtraction of the average velocity and vorticity field, showing the wing in horizontal position. The leading edge vortex, bound vortex and velocity deficit behind the wing are indicated by black cycles and arrows (*Re*=28,000, *k*=0.3, α_0=4 deg., *y*/*c*=2.45). *Re*, Reynolds number; *k*, reduced frequency; α_0, static angle of attack.

stages, from attached to fully separated flow, depending on the spanwise location as well as the phase of the wingbeat cycle. Flow phenomena such as the bound vortex and the velocity deficit behind the wing were revealed by subtracting the horizontal flow velocity from the vector field. In addition Fig. 8 shows a fully developed LEV characterized by the reverse flow direction close to the upper surface.

Fig. 9 shows the instantaneous flow field at four different locations along the span, measured while the wing was passing through the horizontal position during the downstroke (*Re*=28,000, *k*=0.2 and α_0=8 deg.). At a mid-span position (*y*=1.74*c*), the vorticity and vector fields show a small area of separation at the leading edge with reattachment shortly afterwards (Fig. 9A). While the flow was still mainly attached at a slightly more distal mid-span position (*y*=2.04*c*), a large vortex-like structure was evident on the upper surface beginning at the leading edge and stretching over approximately 2/3 of the chord. The vorticity region clearly shows reverse flow close to the surface; i.e. the vorticity region is clearly defined and the flow reattaches shortly afterwards (Fig. 9B). The two distal locations showed different stages of flow separation. The slightly more proximal position (*y*=2.45*c*) revealed the shedding of a distinct vortex structure in addition to a second vortex structure at the leading edge (Fig. 9C). Meanwhile at location closest to the tip (*y*=2.80*c*), the flow was fully separated beginning at the leading edge (Fig. 9D).

The reduced frequency and Reynolds number dependency of the flow fields at the horizontal downstroke position and close to the lower reversal point is shown at a distal span location (*y*=2.45*c*) in Fig. 10. At *k*=0.2 the flow changed from a near-wall separation while passing the horizontal position (Fig. 10A) into fully separated flow when approaching the lower reversal point (Fig. 10B). At a lower reduced frequency, *k*=0.1, the flow field showed a clear separation at the leading edge and a vortical structure above the wing at the horizontal position. The vortex was limited to the chord length and clearly attached to the surface with its core approximately at 1/3 of the chord length (Fig. 10C). Similar to *k*=0.2, the flow field exhibited fully separated flow conditions when approaching the lower reversal point (Fig. 10D). For *k*=0.05, a very small separation at the LEV is indicated by the vector field at the horizontal position, but it is not possible to discern the vorticity at the displayed scale (Fig. 10E). A distinct and localized LEV appeared near the lower reversal point very much in contrast to the separated flow conditions at higher *k* (Fig. 10F).

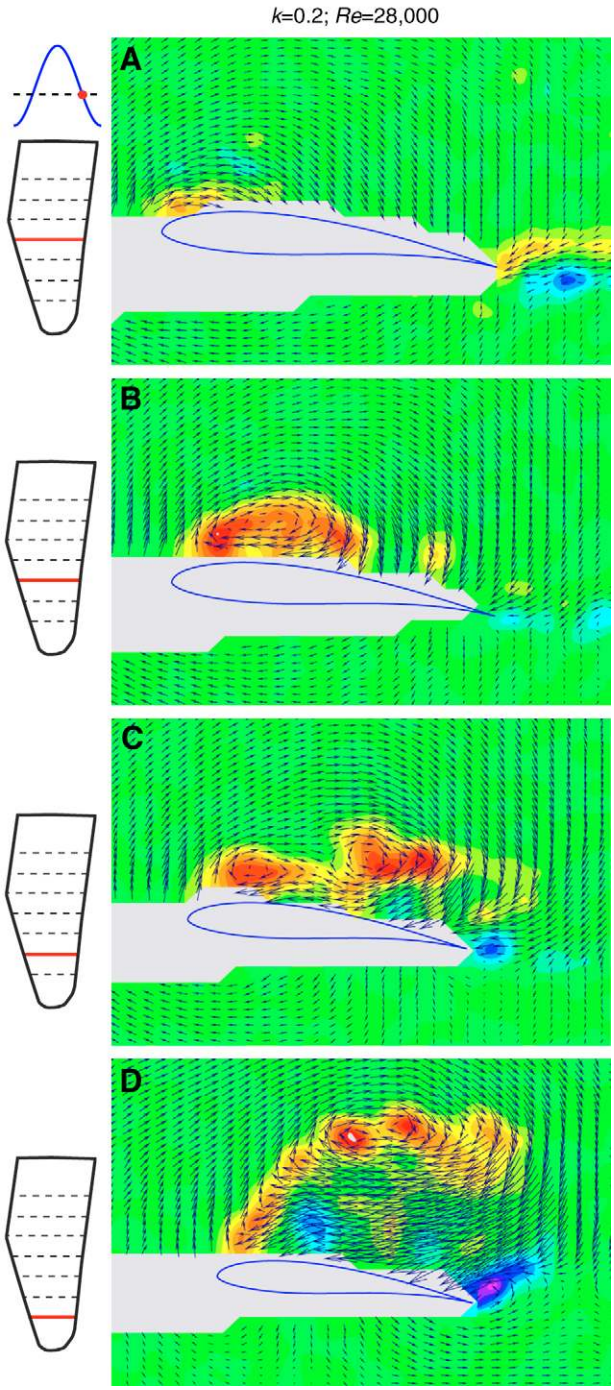

Fig. 9. Vector and vorticity fields showing the flow at different positions along the span during mid downstroke. (A) *y*/*c*=1.74; (B) *y*/*c*=2.09; (C) *y*/*c*=2.45; (D) *y*/*c*=2.80. (*Re*=28,000, *k*=0.2, α_0=8 deg., θ=0 deg.) *Re*, Reynolds number; *k*, reduced frequency; α_0, static angle of attack.

Different flow conditions could be observed at the same spanwise location over different phases of the lower part of the wingbeat cycle for *k*=0.3 (Fig. 11). The first step towards fully separated flow at the leading edge was recorded going through the horizontal position (Fig. 11A). Approaching the lower reversal point, the previously more organized flow structure changed into a fully separated state (Fig. 11B). At the lower reversal point and the beginning of the upstroke, the upper surface showed marginally separated flow, in

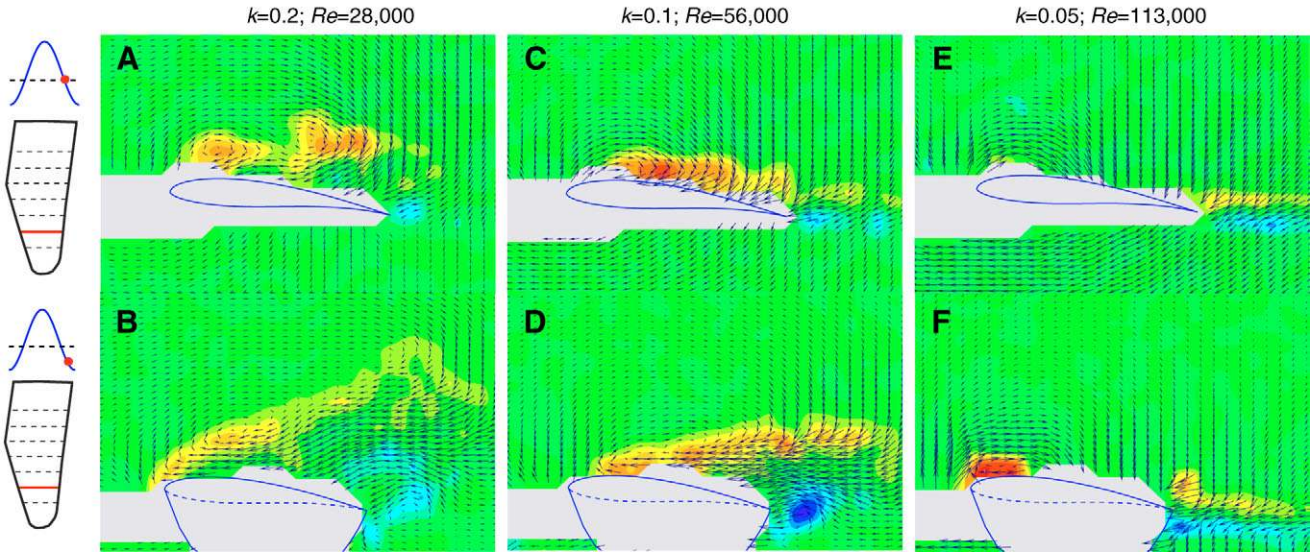

Fig. 10. Vector and vorticity fields showing the flow conditions at half-span position *y*/*c*=2.45 for two positions during the downstroke, θ=0 deg. and θ=–10 deg. at different reduced frequencies (*k*) and *Reynolds numbers* (*Re*) (with a static angle of attack of α_0=8 deg.). θ, amplitude angle.

the form of a shear layer riding on top of the surface. Approaching the horizontal position during the upstroke, the flow started separating on the lower surface, building a small separation bubble starting at approximately 1/4 of the chord length. Meanwhile the upper surface vorticity layer was still present (Fig. 11C). Shortly after, just past the horizontal position, the upper surface vorticity layer had disappeared while the separation bubble on the lower surface had developed into a full LEV with a reverse-flow region and starting directly at the leading edge (Fig. 11D).

DISCUSSION

Although it is well known that quasi-steady assumptions do not correctly predict the force generation of insect wings (Ellington, 1984) and that unsteady effects such as delayed stall can contribute up to 2/3 of the required lift generation for insects (van den Berg and Ellington, 1997), bird flight is still often treated as quasi-steady due to its low reduced frequencies (Pennycuick, 1968; Rayner, 1979; Tobalske et al., 2003). Our results demonstrate that even at the relatively low reduced frequencies of large animal flight, unsteady effects can nevertheless be an important force to reckon with. Although it has been suggested that LEVs may arise during bird flight, it has usually been assumed that they are present only in extreme circumstances, such as the hovering of hummingbirds and the highly swept wings of swifts. So far LEVs have been observed in wind tunnel studies of static wings of model and real swifts (Videler et al., 2004; Lentink et al., 2007). The Reynolds number of gliding swifts has been reported to be at 37,500 (Bruderer and Boldt, 2001), considerably lower than those calculated for medium-sized geese during migration (*Re*=158,000), nonetheless within our lower measurement range. For sufficiently high sweep angles (40–50 deg.) LEVs were present for Reynolds numbers of 12,000–77,000; however, contrary to our results these were not accompanied by higher lift coefficients (Lentink et al., 2007). Recent studies of swifts during cruise (Henningsson et al., 2008) have focused on the flow in the wake rather than on the wing itself, and so LEVs have yet to be visualized in swift flapping flight. LEVs have been shown to be present in the flight of hovering hummingbirds; however, the LEV is inconsistent in its strength and qualitatively different from that known in insect flight, contributing far less to the overall lift generation (Warrick et al., 2009). Our results from a simplified goose-like model show that, in the flight regime of large birds, dynamic stall is a force that has to be carefully considered. Although we are operating at relatively low reduced frequencies and with a rounded leading edge profile [both of which would tend to discourage the development of LEVs (Ellington, 2006)], the influence of the dynamic stall effect and flow separation were clearly visible in both the results of vertical and horizontal force coefficients as well as the PIV measurements.

The development of the vertical force coefficient over the wingbeat cycle showed the influence of strong unsteady flow effects. Under conditions with sufficiently high effective angles of attack, the maximum vertical force coefficient for flapping wings significantly exceeded the maximum vertical force coefficient measured for fixed wings over Reynolds numbers ranging from 28,000 to 133,000, with values between 56% and 7%. This stands in contrast to the low lift performance measured for wings attached to a propeller rig at *Re* 20,000–50,000 (Ellington and Usherwood, 2001), generating maximum lift coefficients around 0.8 compared with values of 1.75 found under ‘Hawkmoth’ flight conditions [*Re*=8000 (Usherwood and Ellington, 2002a)]. However, our findings, with maximum vertical force coefficients well over 1 (C_{z_max}<1.3), are in good agreement with measurements on quail wings at *Re*=26,000 with maximum vertical force coefficient values between 1.5 and 2 (Usherwood and Ellington, 2002b).

Our results suggest that a LEV developed on the upper surface, increasing the lift well above the maximum force coefficient for fixed wings. The significant drop in the vertical force coefficients at high reduced frequencies while approaching the mid-downstroke position suggests that for high effective angle of attacks, flow separation occurred at the distal part of the wing, and is most probably enhanced by the breakdown and shedding of the LEV, resulting in a distinctive hysteresis loop at Reynolds numbers between 28,000 and 56,000 (Fig. 5). One has to keep in mind that different flow conditions occur simultaneously along the span (Fig. 9), and that all of these conditions contribute to the resulting

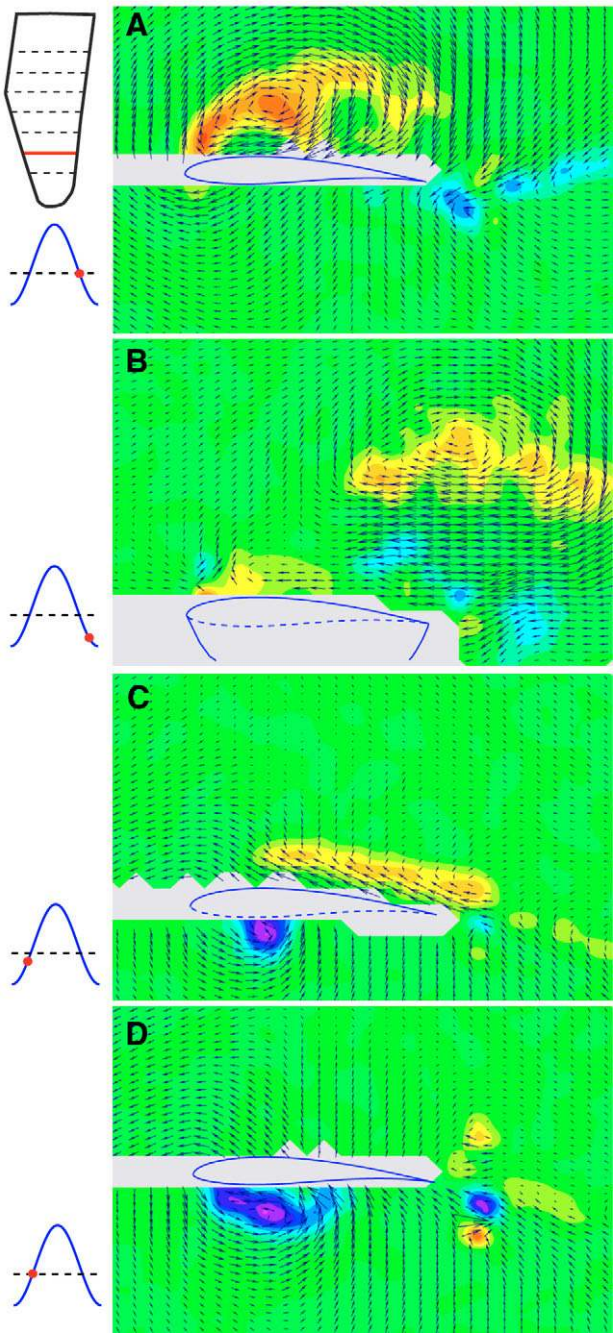

Fig. 11. Vector and vorticity fields showing the flow development during parts of down- and upstroke at distal wing position y/c=2.45. (A) Mid-downstroke (θ=0 deg.), (B) close to lower reversal point (θ=–12 deg.), (C) upstroke close to horizontal position (θ=–4 deg.), (D) mid-upstroke (θ=0 deg.). *Re*=28,000, *k*=0.3, α_0=4 deg. *Re*, Reynolds number; *k*, reduced frequency; α_0, static angle of attack; θ, amplitude angle.

force measured on the model. Lift enhancement due to LEV development at mid-span position could be damped or cancelled out by regions of flow separation at distal wing locations, and while prevailing flow conditions were clearly reflected in the force measurements, it was impossible to determine the local conditions or the state of the LEV development from the force measurements alone. However, using the conditions observed along the span at different phases of the wingbeat cycle as a guide, we can speculate about the reasons for the different features seen in the force measurements.

'Transition stages' were observed in-between the separated regions at the leading edge, LEVs and fully separated flow. Depending on the flight parameters, spanwise location and wingbeat phases, the LEV size varied greatly, varying from a locally contained structure at the leading edge to long layers of vorticity stretched along the entire upper surface. In addition, the shedding of discrete LEVs close to the upper surface was observed at some spanwise positions, and located at times in-between the LEV appearance and the onset of fully separated flow. The LEV detached and shed as a discrete vortex, while a secondary vortex structure appeared, located in the leading edge region. The shedding of LEVs, as observed in the PIV images, is closely correlated to an increase in drag and sudden drop in lift generation, as indicated by the hysteresis loop of the vertical force coefficient *versus* angle of attack (McCroskey, 1981; Daley and Jumper, 1984). These LEV typical features – an increase in lift above maximum vertical force coefficient values for flapping wings followed by a sudden drop at very high angles of attack, as well as in the abrupt increase in horizontal force – were also clearly visible in the force measurements at high reduced frequencies (Figs 5 and 7). In addition, the appearance of secondary and tertiary vortices has been reported to occur during the shedding of the primary LEV, and these are associated with further fluctuations in the aerodynamic forces (McCroskey, 1981). While these fluctuations were not detectable in the present force measurements (which might be explained by the 3-D movement and associated damping effects), the shedding of what appeared to be an 'old' LEV in the presence of a secondary still-attached vortex was a reoccurring theme observed at several spanwise locations and phases of the wingbeat cycle.

Additional flow phenomena were observed during the lower part of the wingbeat cycle between the time that wings were horizontal on the downstroke, and when they were horizontal during upstroke. Their occurrence and intensity varied with spanwise position, reduced frequency and Reynolds number. In the chosen example (Fig. 11) the supposedly pre-existing LEV was in the process of separation during the passing of the horizontal position during the downstroke and transformed into a fully separated flow while approaching the lower reversal point. Due to the sinusoidal-like motion of the wing, the wings lingered around the reversal points and a change in flow condition could be observed. Fully separated upon arrival at the lower reversal point, the flow at the upper surface became only marginally separated by the beginning of the upstroke. Simultaneously, a LEV formed on the lower surface and the shear layer riding on top of the surface disappeared. This might provide an explanation for vertical force coefficients that exceeded the fixed wing values at the beginning of the upstroke but were lower during the second half, as seen in Fig. 5 at *Re*=28,000. The shear layer of positive vorticity along the surface represents nearly ideal conditions for lift generation; almost separated, it generates a large low-pressure region right along the surface without leaving the trailing edge (Lissaman, 2003). The development of the lower surface LEV however suggests a drop in force coefficient as the wing approaches the horizontal position at the upstroke. Based on the strong differences in vertical force coefficient values at identical effective angles of attack during the up- and downstrokes, one can conclude that the flow conditions on the wing did not solely depend on the effective angle of attack but that the conditions were heavily influenced by the flow history.

Contrary to insect flight with stable LEVs, the goose model results showed a strong tendency to change from LEV to flow

separation, resulting in increasing horizontal force coefficients and a drop in vertical force generation. The mechanisms that stabilize the LEVs observed under insect flight conditions and keep them attached to the surface have proven to be difficult to identify and might depend on Reynolds number. Previously, spanwise flow due to centrifugal acceleration and spiral vortex structures similar to those formed on delta wings were suspected as mechanisms that limit the growth of LEVs (Ellington et al., 1996; van den Berg and Ellington, 1997). However, neither the strength nor stability of the LEV was affected by the installation of fences to block spanwise flow, introducing an additional theory of limited effective angles of attack due to the downward flow induced by the tip vortex (Birch and Dickinson, 2001). The low lift performance of purely translating wings caused by rapid LEV detachment (Dickinson and Götz, 1993; Lentink and Dickinson, 2009), stands in contrast to this explanation, eliminating the tip vortices as the main cause of stabilization. Recent work (Lentink, 2008; Lentink and Dickinson, 2009) has identified Coriolis and centripetal acceleration as a possible source of LEV stabilization, proposing the independence of LEV stability on Reynolds number at least in the range of insect flight ($100<Re<14{,}000$). However, this explanation is in contrast to earlier presumptions of Reynolds-number-related structural differences in LEVs (Birch et al., 2004). Lentink's work reveals the correlation of LEV stability and the Rossby number (*Ro*), which is proportional to the inverse of Coriolis and centripetal acceleration (Lentink, 2008; Lentink and Dickinson, 2009). The Rossby number compares the degree of translational *versus* rotational wing movement, and can be calculated based on the advance ratio (*J*), wing chord (*c*) and wing length (*R*) in the following manner (Lentink, 2008):

$$Ro = \sqrt{J^2 + 1}\,\frac{R}{c}\ , \tag{2}$$

with

$$J = \frac{\mathbf{U}_\infty}{4Af}\ , \tag{3}$$

where *A* is the total amplitude in meters and *f* is the flapping frequency. In hovering flight, with no free-stream velocity, advance ratio equals zero and Rossby number is solely based on the chord-to-wing length ratio. By contrast, in forward flight, advance ratio contributes significantly to Rossby number. For our model at Re=28,000 and k=0.3 we calculated an advance ratio of 4.3 and a Rossby number of 15, which is significantly higher than $Ro<0.3$ typical for hovering flight of insects, bats and birds (Lentink and Dickinson, 2009). This very high value of the Rossby number supports the easy transition between LEV and stall condition observed with our model.

The investigation of the simplified flapping wing model shows the potential impact of stall and delayed stall flow conditions on vertebrate flight. One has to contemplate the importance that biological wing deformation, morphology and kinematic refinements hold in order to alter the aerodynamic performance of the wing. However, almost nothing is known about optimum kinematics, profiles, wing torsion, surface roughness and other parameters in bird flight. Animal wings can deform considerably over the course of a wingbeat cycle (Swartz et al., 1996; Swartz et al., 2007; Walker et al., 2009; Walker et al., 2010). Passive deformation due to aerodynamic and inertial forces dominates on membrane wings such as that seen in insect and bat flight, and recent work explores the effect of wing compliance on the aerodynamic performance of the wings. Changing the camber, twist and trailing edge flexibility on insect wings showed an improved performance for compliant insect wings compared with rigid wings (Young et al., 2009; Zhao et al., 2009). The improved performance of compliant wings with higher lift slopes, greater force magnitude and higher critical angles of attack also applies to bat flight (Song et al., 2008; Waldman et al., 2008). Little is known about the extent of active or passive wing deformation in bird flight; however, distinct differences were found in the profile of flying and anesthetized or dead animals (Biesel et al., 1985; Brill, 1992). In addition to changes in camber, twist and bending due to wing deformation, additional kinematic parameters such as span variation, stroke plane angle, supination and pronation can be changed over the course of a wingbeat cycle with profound effects on the aerodynamics (Hedrick et al., 2002; Tobalske et al., 2007; Hubel et al., 2009) (T.Y.H., D. K. Riskin, S. M. Swartz and K. S. Breuer, submitted).

Flow conditions such as stall and LEV development will largely be influenced by these parameters, especially by the difference in the effective angle of attack along the span of real bird wings compared with the model. The ability to twist the wing in spanwise direction reduces the incidence towards the wingtip compared with an untwisted wing. One can assume that negative lift coefficients as well as leading edge separation during the upstroke, as found in the simplified model, will probably be suppressed and not be present in real flying birds due to these morphological and kinematic adjustments.

For future work it is suggested to investigate the influence of different parameters on the stall and LEV development on the wing. Starting with relatively simple changes such as the implementation of a sharp leading edge which is most probably critical to the LEV development, supporting the onset of the leading edge flow separation necessary to create the LEV (Ellington, 2006). We also predict the sharp leading edge to act as a turbulator causing an earlier flow transition that will influence the results at Re=28,000 considerably.

More complex alteration could include changes in the flexibility of the wings as well as active longitudinal rotation and changes in wing extension over the wingbeat cycle. Furthermore, one might consider the effects of surface roughness and the use of real bird wings.

Conclusions

Our investigation shows that LEVs, as well as other flow phenomena based on the flapping motion clearly occur on a simplified flapping model operating in the range of Reynolds numbers and reduced frequencies typical for vertebrate flight. We have identified a variety of different flow conditions depending on the spanwise location and wingbeat phase. The strength and occurrence of flow conditions such as the presence of LEVs and stall depend strongly on Reynolds number and reduced frequency. While the effects of LEV and stall on the vertical force generation might be suppressed due to their simultaneous occurrence along the span, there is a clear deficit in thrust generation due to the LEV and separation effects. In addition, the LEV easily transforms into flow separation, contrary to the stable conditions observed in insect flight.

The ability of animals to control important parameters such as twist, camber and effective angle of attack along the span might be an important key for flight efficiency and control in vertebrate flight. In light of the observed unsteady effects in the force measurements, the significant increase in drag generation, as well as the occurrence of different flow conditions along the span and during the wingbeat cycle, one must address the importance of adaptive wings, and their utility to suppress or stabilize the development of LEVs.

Other future investigations are planned to clarify how a sharp leading edge (typical for the distal part of bird wings) can affect and possibly enhance the frequency of occurrence and the stability of the LEV.

LIST OF SYMBOLS AND ABBREVIATIONS

A	the total amplitude in meters
b	wingspan
c	average wing chord
C_D	drag coefficient
C_L	lift coefficient
C_m	pitching coefficient
C_x	horizontal force coefficient
C_z	vertical force coefficient
$C_{z\_max\_fixed}$	maximum force coefficient for fixed wings
$C_{z\_max\_flap}$	maximum vertical force coefficient for flapping wings
f	wingbeat frequency
J	advanced ratio
k	reduced frequency
LEV	leading edge vortex
p	precision range
PIV	particle image velocimetry
r	measurement range
R	length of one wing
Re	Reynolds number
Ro	Rossby number
$\mathbf{U}_\infty$	free-stream velocity
$\mathbf{v}_z$	vertical component of wing velocity
α_0	static angle of attack
α_{eff}	effective angle of attack
α_{ind}	induced angle of attack
θ	amplitude angle

ACKNOWLEDGEMENTS

We thank E. Stamhuis for helpful discussions in the process of data collection and W. Thielicke for his contribution in the data analysis process. We are grateful to K. Breuer and D. Lentink for the opportunity to discuss this work in detail and helpful suggestions regarding the manuscript. This work was funded by the DFG (Deutsche Forschungsgemeinschaft) through grant TR 194/26.

REFERENCES

Althaus, D. (1981). *Stuttgarter Profilkatalog.* Braunschweig: F. Vieweg.
Altshuler, D. L., Dudley, R. and Ellington, C. P. (2004). Aerodynamic forces of revolving hummingbird wings and wing models. *J. Zool.* **264**, 327-332.
Biesel, W., Butz, H. and Nachtigall, W. (1985). Einsatz spezieller Verfahren der Windkanaltechnik zur Untersuchung des freien Gleitflugs von Vögeln. In *BIONA Report 3*, pp. 109-122. Stuttgart: Gustav Fischer Verlag.
Bilo, D. (1971). Flugbiophysik von Kleinvögeln. I. Kinematik und Aerodynamik des Flügelabschlages beim Haussperling (*Passer domesticus* L.). *Z. Vergl. Physiol.* **71**, 382-454.
Bilo, D. and Nachtigall, W. (1977). Biophysics of bird flight: questions and results. *Fortschr. Zool.* **24**, 217-234.
Birch, J. M. and Dickinson, M. H. (2001). Spanwise flow and the attachment of the leading-edge vortex on insect wings. *Nature* **412**, 729-733.
Birch, J. M., Dickson, W. B. and Dickinson, M. H. (2004). Force production and flow structure of the leading edge vortex on flapping wings at high and low Reynolds numbers. *J. Exp. Biol.* **207**, 1063-1072.
Brill, C. (1992). *Stereophotogrammetrische Untersuchungen zur Konfiguration des Rumpfes und der auftriebserzeugenden Flächen eines im Windkanal gleitfliegenden Stares (Sturnus vulgaris L.).* Saarbrücken: Universität des Saarlandes.
Bruderer, B. and Boldt, A. (2001). Flight characteristics of birds. *Ibis* **143**, 178-204.
Butler, P. J. and Woakes, A. J. (1980). Heart-rate, respiratory frequency and wing beat frequency of free flying barnacle geese *branta-leucopsis*. *J. Exp. Biol.* **85**, 213-226.
Cuvelier, F. (2000). *Voisin des Nuages avec les Oies Sauvages.* France: ARTE France.
Daley, D. C. and Jumper, E. J. (1984). Experimental investigation of dynamic stall for a pitching airfoil. *J. Aircraft* **21**, 831-832.
Dickinson, M. H. and Götz, K. G. (1993). Unsteady aerodynamic performance of model wings at low Reynolds numbers. *J. Exp. Biol.* **174**, 45-64.
Dickinson, M. H., Lehmann, F. and Sane, S. P. (1999). Wing rotation and the aerodynamic basis of insect flight. *Science* **284**, 1954-1960.
Ellington, C. P. (1984). The aerodynamics of hovering insect flight. I. The quasi-steady analysis. *Philos. Trans. R. Soc. Lond. B. Biol. Sci.* **305**, 1-15.
Ellington, C. P. (1999). The novel aerodynamics of insect flight: applications to micro-air vehicles. *J. Exp. Biol.* **202**, 3439-3448.
Ellington, C. P. (2006). Insects versus birds: the great divide. *44th AIAA Aerospace Sciences Meeting and Exhibit*, pp. 1-6.
Ellington, C. P. and Usherwood, J. R. (2001). Lift and drag characteristics of rotary and flapping wings. In *Fixed and Flapping Wing Aerodynamics for Micro Air Vehicle Applications*, vol. 195 (ed. T. J. Mueller), pp. 231-248. Reston: AIAA.
Ellington, C. P., van den Berg, C., Willmott, A. P. and Thomas, A. L. R. (1996). Leading-edge vortices in insect flight. *Nature* **384**, 626-630.
Green, M. and Alerstam, T. (2000). Flight speeds and climb rates of Brent Geese: mass-dependent differences between spring and autumn migration. *J. Avian Biol.* **31**, 215-225.
Hedenström, A., Rosén, M. and Spedding, G. R. (2006). Vortex wakes generated by robins *Erithacus rubecula* during free flight in a wind tunnel. *J. R. Soc. Interface* **3**, 263-276.
Hedenström, A., Johansson, L. C., Wolf, M., von Busse, R., Winter, Y. and Spedding, G. R. (2007). Bat flight generates complex aerodynamic tracks. *Science* **316**, 894-897.
Hedrick, T. L., Tobalske, B. W. and Biewener, A. A. (2002). Estimates of circulation and gait change based on a three-dimensional kinematic analysis of flight in cockatiels (*Nymphicus hollandicus*) and ringed turtle-doves (*Streptopelia risoria*). *J. Exp. Biol.* **205**, 1389-1409.
Hedrick, T. L., Usherwood, J. R. and Biewener, A. A. (2004). Wing inertia and whole-body acceleration: an analysis of instantaneous aerodynamic force production in cockatiels (*Nymphicus hollandicus*) flying across a range of speeds. *J. Exp. Biol.* **207**, 1689-1702.
Hedrick, T. L., Cheng, B. and Deng, X. (2009). Wingbeat time and the scaling of passive rotational damping in flapping flight. *Science* **324**, 252-255.
Henningsson, P., Spedding, G. R. and Hedenström, A. (2008). Vortex wake and flight kinematics of a swift in cruising flight in a wind tunnel. *J. Exp. Biol.* **211**, 717-730.
Hubel, T. and Tropea, C. (2009). Experimental investigation of a flapping wing model. *Exp. Fluids* **46**, 945-961.
Hubel, T. Y., Hristov, N., Swartz, S. M. and Breuer, K. S. (2009). Time-resolved wake structure and kinematics of bat flight. *Exp. Fluids* **46**, 933-943.
Iriarte-Diaz, J. and Swartz, S. M. (2008). Kinematics of slow turn maneuvering in the fruit bat *Cynopterus brachyotis*. *J. Exp. Biol.* **211**, 3478-3489.
Lee, S. Y., Scott, G. R. and Milsom, W. K. (2008). Have wing morphology or flight kinematics evolved for extreme high altitude migration in the bar-headed goose? *Comp. Biochem. Physiol. C Pharmicol. Toxicol. Endocrinol.* **148**, 324-331.
Lentink, D. (2008). Exploring the biofluiddynamics of swimming and flight. PhD thesis. Experimental Zoology Group, Wageningen.
Lentink, D. and Dickinson, M. H. (2009). Rotational accelerations stabilize leading edge vortices on revolving fly wings. *J. Exp. Biol.* **212**, 2705-2719.
Lentink, D., Muller, U. K., Stamhuis, E. J., de Kat, R., van Gestel, W., Veldhuis, L. L. M., Henningsson, P., Hedenstrom, A., Videler, J. J. and van Leeuwen, J. L. (2007). How swifts control their glide performance with morphing wings. *Nature* **446**, 1082-1085.
Lissaman, P. B. S. (2003). Low-reynolds-number airfoils. *Annu. Rev. Fluid Mech.* **15**, 223-239.
McCroskey, W. J. (1981). The phenomenon of Dynamic Stall. *NASA TM-81264*.
Muijres, F. T., Johansson, L. C., Barfield, R., Wolf, M., Spedding, G. R. and Hedenström, A. (2008). Leading-edge vortex improves lift in slow-flying bats. *Science* **319**, 1250-1253.
Pennycuick, C. J. (1968). Power requirements for horizontal flight in the pigeon *Columba livia*. *J. Exp. Biol.* **49**, 527-555.
Perrin, J. (2001). *Winged Migration.* France: Sony Pictures Classics.
Rayner, J. M. V. (1979). A vortex theory of animal flight. Part 2. The forward flight of birds. *J. Fluid Mech.* **91**, 731-763.
Rayner, J. M. V. (1999). Estimating power curves of flying vertebrates. *J. Exp. Biol.* **202**, 3449-3461.
Riskin, D. K., Willis, D. J., Iriarte-Díaz, J., Hedrick, T. L., Kostandov, M., Chen, J., Laidlaw, D. H., Breuer, K. S. and Swartz, S. M. (2008). Quantifying the complexity of bat wing kinematics. *J. Theor. Biol.* **254**, 604-615.
Rosen, M., Spedding, G. R. and Hedenstrom, A. (2004). The relationship between wingbeat kinematics and vortex wake of a thrush nightingale. *J. Exp. Biol.* **207**, 4255-4268.
Sane, S. P. (2003). The aerodynamics of insect flight. *J. Exp. Biol.* **206**, 4191-4208.
Song, A., Xiaodong, T., Israeli, E., Galvao, R., Bishop, K., Swartz, S. M. and Breuer, K. S. (2008). Aeromechanics of membrane wings with implications for animal flight. *AIAA J.* **46**, 2096-2106.
Spedding, G. R. (1993). On the significance of unsteady effects in the aerodynamic performance of flying animals. *Contemp. Math.* **141**, 401-419.
Spedding, G. R., Rosen, M. and Hedenström, A. (2003). A family of vortex wakes generated by a thrush nightingale in free flight in a wind tunnel over its entire natural range of flight speeds. *J. Exp. Biol.* **206**, 2313-2344.
Swartz, S. M. and Middleton, K. M. (2008). Biomechanics of the bat limb skeleton: scaling, material properties and mechanics *Cells Tissues Organs* **187**, 59-84.
Swartz, S. M., Groves, M. S., Kim, H. D. and Walsh, W. R. (1996). Mechanical properties of bat wing membrane skin. *J. Zool.* **239**, 357-378.
Swartz, S. M., Diaz, J., Riskin, D. K., Song, A., Tian, X., Willis, D. J. and Breuer, K. S. (2007). Wing structure and the aerodynamic basis of flight in bats. In *Proceedings of AIAA Aerospace Science Meeting, Reno NV. January 2007*.
Tobalske, B. W. (2007). Biomechanics of bird flight. *J. Exp. Biol.* **210**, 3135-3146.
Tobalske, B. W., Hedrick, T. L., Dial, K. P. and Biewener, A. A. (2003). Comparative power curves in bird flight. *Nature* **421**, 363-366.
Tobalske, B. W., Warrick, D. R., Clark, C. J., Powers, D. R., Hedrick, T. L., Hyder, G. A. and Biewener, A. A. (2007). Three-dimensional kinematics of hummingbird flight. *J. Exp. Biol.* **210**, 2368-2382.
Usherwood, J. R. and Ellington, C. P. (2002a). The aerodynamics of revolving wings I. Model hawkmoth wings. *J. Exp. Biol.* **205**, 1547-1564.

Usherwood, J. R. and Ellington, C. P. (2002b). The aerodynamics of revolving wings II. Propeller force coefficients from mayfly to quail. *J. Exp. Biol.* **205**, 1565-1576.
van den Berg, C. and Ellington, C. P. (1997). The three-dimensional leading-edge vortex of a 'hovering' model hawkmoth. *Philos. Trans. R. Soc. B. Biol. Sci.* **352**, 329-340.
Videler, J. (2005). *Avian Flight.* Oxford: Oxford University Press.
Videler, J., Stamhuis, E. and Povel, D. (2004). Leading-edge vortex lifts swifts. *Science* **306**, 1960-1962.
Waldman, R. M., Song, A., Riskin, D. K., Swartz, S. M. and Breuer, K. S. (2008). Aerodynamic behavior of compliant membranes as related to bat flight. In *AIAA Fluid Dynamics Conference.* Seattle, WA.
Walker, S. M., Thomas, A. L. R. and Taylor, G. K. (2009). Deformable wing kinematics in the desert locust: how and why do camber, twist and topography vary through the stroke? *J. R. Soc. Interface* **6**, 735-747.
Walker, S. M., Thomas, A. L. R. and Taylor, G. K. (2010). Deformable wing kinematics in free-flying hoverflies. *J. R. Soc. Interface* **7**, 131-142.
Warrick, D. R., Tobalske, B. W. and Powers, D. R. (2005). Aerodynamics of the hovering hummingbird. *Nature* **435**, 1094-1097.
Warrick, D. R., Tobalske, B. W. and Powers, D. R. (2009). Lift production in the hovering hummingbird. *Proc. R. Soc. B. Biol. Sci.* **276**, 3747-3752.
Willmott, A. P., Ellington, C. P. and Thomas, A. L. R. (1997). Flow visualization and unsteady aerodynamics in the flight of the hawkmoth, *Manduca sexta. Philos. Trans. R. Soc. B. Biol. Sci.* **352**, 303-316.
Young, J., Walker, S. M., Bomphrey, R. J., Taylor, G. K. and Thomas, A. L. R. (2009). Details of insect wing design and deformation enhance aerodynamic function and flight efficiency. *Science* **325**, 1549-1552.
Zhao, L., Huang, Q., Deng, X. and Sane, S. P. (2009). Aerodynamic effects of flexibility in flapping wings. *J. R. Soc. Interface.* **7**, 485-497.